LUND UNIVERSITY

Measuring resistivity in a contactless fashion

Author: Jim Klintrup

Thesis submitted for the degree of Bachelor of Science
Project duration: 2 months equivalent

Supervised by Elizabeth Blackburn

Department of Physics
Division of Synchrotron Radiation Physics
May 2020

Abstract

The aim of this thesis work was to develop a rig to measure the resistivity of a metal sample. The initial testing of the rig would be done at room temperature and calibration of the setup would be done with aluminum samples and then metallic alloys would be studied.

The method implemented is a contactless one where the diffusion of eddy currents in a sample is measured by a coil and the resistivity can be deduced. The eddy currents are induced by a pulsed magnetic field and the diffusion of the currents in the sample is due to the resistance of the sample material. This method is the same as that described by C.P. Bean in 1959.

To facilitate the construction of the coils, a coil winding rig was designed and built. In conjunction with this, calculations were made to approximate the resonant circuitry to simplify tuning of that circuitry at a later stage.

Once the preliminary measuring rig was set up, extensive testing, configuration and calibration of the rig was conducted. This was done with and without a test sample of aluminum rod present inside the rig. The goal of this was to eliminate unwanted interference between different components involved in the experiment and to resolve the measurement of the diffusing eddy currents.

In this thesis, limiting factors of the functionality of the experiment setup are explored. The induction of eddy currents in the sample is strongly dependent on the amount of magnetic flux and its rapid change. The change in magnetic field density, going from maximum to zero, took place over the course of microseconds, which was fast enough but the maximum field strength seen was to small to induce sufficient eddy currents for reliable measurements.

Contents

Abbreviations

DSC - Differential Secondary Coil
PE - Polyethylene
PVC - Polyvinyl chloride
CSV - Comma Separated Values

1 Introduction

The scientific aim of this thesis work is to develop a contactless probe for measuring the resistivity of metals. The design of the probe was inspired by the work of C.P. Bean [1], which may be used at room temperature but can also be used at low temperatures in a cryostat.

1.1 Resistivity

Electrical resistivity, ρ, is a property of a material and is the inverse of electrical conductivity, σ, as described by Hofmann [2] (p.79-81) and Griffiths [3] (p. 296-298). Resistivity is defined as the resistance length, Ω·m and with that the resistance, R, of a sample can be calculated using the following formula as outlined by Griffiths [3] (p. 296-298)

$$R = \rho \frac{l}{A} \tag{1}$$

where l is the length and A is the cross-sectional area of the sample.
When a voltage potential difference is applied to a conductor, the electrons flow in a current due to the electric field arising from the potential difference. The electrons in the current interact or scatter with phonons and impurities, giving rise to resistance, and hence resistivity.
Phonons are so-called quasiparticles that are the result of the atoms in a solid thermally oscillating about their time-average equilibrium position, in the crystal structure [2] (p. 68). These oscillations couple, giving rise to collective vibrational modes that can be modeled as waves propagating through the solid. The electrons can interact with these waves, disrupting the path of the current flow. The other contribution to resistance originates from imperfections in the physical structure of the solid, the lattice. These imperfections are usually called impurities and include vacancies, dislocations, interstitial atoms and what they have in common is that they break the symmetry of the lattice.
The theoretical resistivity of a solid metal is the sum the individual contributions to the resistivity. In our case, the two major contributions are from the impurities and from the phonons [2] (p. 204), Equation 2. To a first approximation, the contribution from impurities is temperature independent.

$$\rho(T) = \rho_{\text{ impurities}} + \rho_{\text{ phonons}}(T) \tag{2}$$

In Figure 1, it is illustrated how these two contributions to the resistivity define the overall resistivity. Starting from high temperature, the resistivity has a linear

dependence on temperature and is dominated by the contributions from phonons. Lowering the temperature consequently lowers the resistivity but only to the point where the phonons can be disregarded as the excited population dwindles and the resistivity settles on a constant value related to the impurities in the metal.
The number of phonons, N_p, follows a Bose-Einstein distribution which is dependent on the temperature, T. Equation 3 shows such a distribution where E is the phonon energy and k_B is the Boltzmann constant. It can be shown that this distribution behaves linearly with high temperature and goes to zero for low temperature.

$$N_p = \frac{1}{e^{E/k_B T} - 1} \tag{3}$$

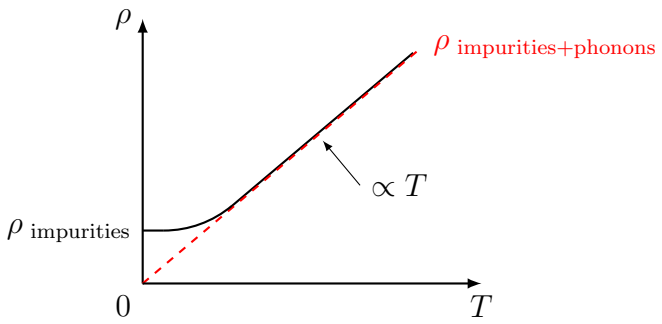

Figure 1: Theoretical model of the resistivity contributions from impurities and phonons in a conductive material as a function of temperature, T. The resistivity is proportional to temperature at high temperatures and converges to a constant value at low enough temperature related to the impurities.

Other contributions to the resistivity, such as from magnetoresistance or electron-electron interactions, are possible, but I neglect these higher order effects here. This model also does not capture the development of superconductivity (for aluminum, superconductivity onsets at 1.2 K [4]; this is outside the scope of this project).

1.2 Measuring resistivity

The resistivity of a material can be used to study the purity or the grade of a given sample. It is common to control the properties of materials using impurities, e.g. aluminum has impurities introduced in order to make it harder and easier to machine.

The evaluation of a material's grade involves measuring the resistivity at a low temperature, low enough that the contributions from phonons to the resistivity are effectively eliminated. This results in the remaining resistivity being dominated by the impurities and the purity can be calculated. Prance [5] used this method to determined the density of hydrogen impurities in niobium discs by measuring the resistivity at high and low temperature, then taking the ratios of those two values, finding the residual resistivity ratios (RRR). This ratio is commonly cited to indicate the quality of a particular sample.
Here follows a survey of some methods used for measuring resistivity.

1.2.1 Contactless methods

The Bean decay method
The method developed by Bean *et al.* [1] is the basis for this project and will be presented first. This method is based on the measurement of decay or diffusion of eddy currents, specifically the eddy currents diffusing in the sample being probed. The magnetic flux dissipation is caused by the diffusion of eddy currents within the sample which decay due to the resistivity as mentioned by Bean *et al.* [1]. The diffusion is described by Bean *et al.* as

$$\frac{\rho}{\mu_0}\nabla^2 B = \frac{\partial B}{\partial t} \tag{4}$$

where μ_0 is vacuum permeability, B is magnetic field density and t is time.
A description of eddy currents is given by Young & Freedman [11] (p. 996) and are described as currents arising as for a changing magnetic field. In this method, the edyy current are induced by a pulse current through the primary coil which surrounds both the sample and a secondary coil. A simple rendering of the setup common to this method is seen in Figure 2; relative sizes and lengths are not to scale.

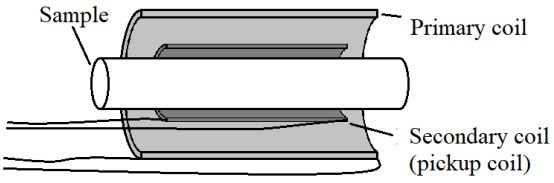

Figure 2: Cross-sectional illustration of the Bean method setup. Sample (white rod) surrounded by secondary coil (dark gray), all surrounded by primary coil (light gray). Relative lengths and sizes not to scale.

The eddy current decay is measured using the secondary coil surrounding the sample, called a pickup coil. The decreasing magnetic flux through the pickup coil generates a voltage differential in the coil, which can be measured. This voltage was established by Bean *et al.* [1] to converge to an exponential

$$V(t) \propto B_0 e^{-t/\tau} \quad \text{where} \quad \tau = G\mu r^2/\rho \tag{5}$$

after a time equal to the time constant τ where μ is the relative permeability of the material, r is the radius of a circular rod in metres, the resistivity is given in Ωm, t is time in seconds and B_0 stands for the initial magnetic field density. The constant G is a geometric factor determined by the coil design, and has a value of $2.17 \cdot 10^{-7}$ sΩ/m.

The time constant τ is found from a solution to the diffusion equation, Equation 4, for a circular cross-section of a infinitely long rod and then the voltage in the pickup coil with N turns is found by integrating the magnetic flux from the diffusion as presented by Bean *et al.* [1].

The measurements aim to find the time constant τ and then use the expression for τ in Equation 5, to ascertain the resistivity.

$$\rho = \frac{G\mu r^2}{\tau} \tag{6}$$

In Equation 6, μ is taken to be approximatly one, $\mu \approx 1$, for non-ferromagnetic materials. Although this calculation was done initially for a long rod, Hartwig *et al.* noted that "Earlier work has shown that cylindrical samples must have a length to diameter ratio (L/D) of greater than eight in order to eliminate end effects" [10] because there are effects at the ends of the rod that can affect the results if the length of the rod is not affected by sufficient magnetic flux. This was also confirmed by LePage *et al.* [13] who suggested that for large length to diameter ratios, L/D ≥ 8, the sample could be considered as infinite. They also found a geometric factor of $2.17 \cdot 10^{-7}$ sΩ/m.

Bean *et al.* used assumptions that are also relevant to this project. One is that the sample is assumed to have isotropic resistivity, meaning that the resistivity is the same throughout the sample. This is a valid assumption as the material I have tested can be considered fairly homogeneous. The method can be adapted to measure the resistivity at different locations when using a pickup coil that is small compared to the sample rod by placing the pickup coil at different positions along the rod, making subsequent measurements and then averaging over those measurements to get a average resistivity.

A second assumption is that the sample material is not ferromagnetic, or at least that the material has a relative magnetic permeability close to one, $\mu \approx 1$. This assumption helps calculations and negates the need to know or measure the magnetic permeability of a material which applies to aluminum with relative permeability of 1.00000065 [12]. Another metal this assumption applies for is copper with relative magnetic permeability of 0.999994 [12].

Magnetic susceptibility

Another method for measuring the resistivity is via the effective magnetic susceptibility of a sample via alternating magnetic fields induced by AC as described by Kraftmakher [7] and Wejgaard & Tomar [8].
The resistivity of a material can be deduced as the magnetic susceptibility depends on it, together with the frequency of the oscillating field. Although this method is reliable in the sense that a alternating magnetic field with a certain frequency and amplitude is easily generated, it has a drawback. At low temperature and using materials that have a low resistivity, the resonant frequency modes of the sample and the coils come closer together and will interfere with the modes that the pickup (measurement) coil, operates at. This is discussed by Kraftmakher in his study using this method [7]. A depiction of the setup used in this method is shown in Figure 3.

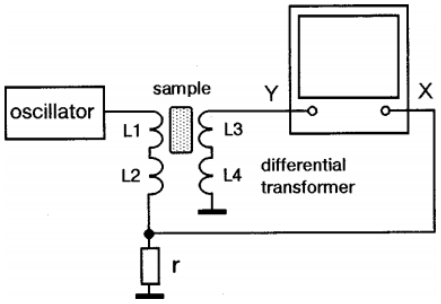

Figure 3: [7] A illustration of the setup used to determine magnetic susceptibility of sample. The oscillator supplies AC to coils L_1 and L_2. Coils L_3 and L_4 pick up diffusing eddy currents from sample. The two pairs of coils connect to the X and Y inputs on oscilloscope, forming the basis for measuring magnetic susceptibility of the sample. The resistor, r, connects to ground.

Magnetization

Finally, one other method is that of measuring the mechanical impulse or torque applied by a rotating magnetic field to a conducting sample. This is discussed in

a article by Delaney & Pippard [9]. The resistivity in this method is determined by measuring the torque generated by the magnetization of the material being probed. From that measurement, the magnetization can be calculated, which is dependent on the resistivity.

1.2.2 4-terminal

For the completeness of this survey, it is worth mentioning the existence of the method based on direct contacts with the sample.
When measuring the resistance of a substance, it is common to use contact leads connected to the ends of a wire or a rod with a method called 4-terminal measurement or 4-wire sensing; a characterization of this is made by Cutkosky [6].
The 4-terminal measurement involves two wires being connected to either end of the sample which are in turn connected to a current source. A second pair of wires are connected adjacent to the first, and are connected to a voltage measuring device. A current is passed through the first pair of wires, generating a voltage drop over the sample which is measured via the second pair of wires, such that the current and voltage are measured independently, and for Ohmic materials the resistance is inferred using Ohm's law, $V = IR$, where V is the voltage drop and I is the current fed through the circuit as discussed by Griffiths [3] (p.296-298).
The method will provide an answer but it will depend on several presumptions. The first difficulty with this method is that the contacts between the leads and the sample must be of very high quality. If these contacts present any resistance of their own, they will influence the measurement and therefore the result.
Another factor to consider is if the substance is fairly homogeneous in its impurity distribution as the current will take the path of least resistance giving a result that is potentially not representative of the average resistance.
Additionally, when considering a situation where the resistivity is expected to be low, the mean free path of the electrons must be taken into account. The mean free path is the concept of the average distance between each electron interaction and is closely related to the resistivity, as Hofmann explains [2] (p. 79-81). This average distance increases with decreasing resistivity and the distance between contacts should always be longer than the mean free path to ensure accurate measurement.

1.3 Circuitry

The measurement of diffusing eddy currents cannot be done simply via the implementation of a electronic circuit. Because the coils have an inductance, capacitance

and a resistance, the entire circuitry can be considered to behave as a RLC-circuit (resistor-inductor-capacitor-circuit).
In order to control the behavior of the RLC-circuit, one needs to introduce a damping resistor to the circuit. The resonant frequency of such a circuit is defined as

$$\omega = \sqrt{\frac{1}{LC}}, \tag{7}$$

where L is the inductance and C is the capacitance, as described by Young & Freedman [11] (p.1060).The inductance for a solenoid is defined as

$$L = \frac{\mu_0 N^2 A}{l}, \tag{8}$$

where μ_0 is the vacuum permeability, N is the number of turns of the coil winding, A is the cross-sectional area of the coil and l is the length of the coil winding.
The capacitance is defined as

$$C = \frac{\epsilon_0 A}{d}, \tag{9}$$

where ϵ_0 is the vacuum permittivity and d is the distance between opposing surfaces.
The inductance and the capacitance of the primary and secondary coil is calculated using Equation 8 and 9 as they are needed in both cases. The capacitance is calculated by assuming that each turn of the coil can be considered as a ring. Each ring has an area equal to the wire width multiplied with the circumference of the ring. The distance between each ring pair is taken as the width of the wire and the accumulative capacitance is found by adding up the capacitance of each neighboring pair.
The critical damping resistor in series and parallel are respectively define as

$$R_{series} = \sqrt{\frac{4L}{C}} \quad \text{and} \quad R_{parallel} = \frac{1}{2}\sqrt{\frac{L}{C}} \quad . \tag{10}$$

which are shown for cases of underdamped oscillation by Young & Freedman [11] (p. 1032-1034).
The time constants for RLC-circuits are $2L/R$ for parallel and $2RC$ for series, Young & Freedman (p.1033). Here, the behavior of the voltage is described by a exponential function $e^{-t/\tau}$ where t is time and τ is the time constant.

$$\text{Parallel: } e^{-t/(2L/R)} \quad \text{Series: } e^{-t/(2RC)} \tag{11}$$

2 Method

2.1 Setup and measurement

The function generator used throughout the experiment was a Seintek G5100 which had a maximum power consumption of 20 W. The maximum current the function generator could supply with its internal resistance of 50 Ω and no external resistance was 0.6 A.
The experiment used a Tektronix DPO 2024 that was able to save screen captures and data from the oscilloscope to file and a software designated Openchoice Desktop App. The data from the oscilloscope was saved as CSV-files (comma separated values) which later was plotted and fitted with a exponential expression in a graphing program to recover and analyze the signal.

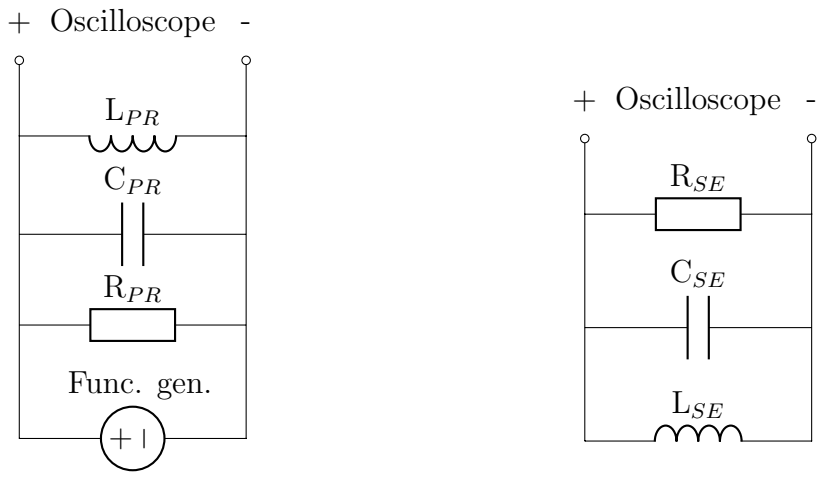

(a) Primary coil circuit. R_{PR} is the primary coil dampening resistor, C_{PR} and L_{PR} are the capacitance and inductance of the primary coil.

(b) Secondary coil circuit. R_{SE} is the secondary coil dampening resistor, C_{SE} and L_{SE} are the capacitance and inductance of the secondary coil.

Figure 4: Equivalent circuits for the primary and secondary coil with all components in parallel.

The schematics of the primary and secondary coil circuitry are presented in Figure 4. During the course of this work, it was found that all components of the RLC-circuit could be considered to be in parallel (see below).
In Table 1, the parameters of each coil are given, and the characteristics of the electronic components are calculated using equations from section 1.3.

Table 1: Specifications for the primary and secondary coils. N is the number of turns of wire on coil, A is the equivalent area of wire for each turn, l is the length of the coil, d is the equivalent distance between each turn and the last column specify the considered amount of wire pairs on the coil.

	N	A [mm^2]	l [mm]	d [mm]	pairs
Primary	265	17.9	90.4	0.3	264
Secondary	77	9.4	25	0.3	76

The inductance of the primary coil was calculated to be 247 μH and the capacitance 0.14 nF which in turn meant that the damping resistor, if in parallel, would be 660 Ω, calculated with Equation 10. The same calculations were made for the secondary coil and found that it had an inductance of 23 μH and capacitance of 21 pF. This in turn gave that the damping resistor for the secondary coil should be 526 Ω. These calculations gave a starting point from which tuning the circuit to the actual damping resistance was made.
The calculations also gave a opportunity to confirm the assumption about the coil circuitry being considered RLC with all of its components in parallel. Using the previously calculated inductance for the primary coil, combined with the use of a 660 Ω damping resistor in parallel it was seen from Equation 11 that the time constant should be ~ 0.7 μs. This corresponds to the amplitude of the voltage being $1/e$ or 0.37 of the peak amplitude, 0.7 μs after the initial pulse. This was confirmed by investigating the voltage response from the primary coil with an oscilloscope; this is discussed in more detail in Section 3.1 and shown in Figure 12(b).

A test Al rod was used to aid the design of the measuring probe. The time constant τ related to aluminum was calculated from the tabulated resistivity of aluminum, $2.7 \cdot 10^{-8}$ Ωm at 20 °C [14], and the definition of τ from Bean *et al.* in Equation 5. The test rod was made using the specifications for future rods to be tested (diameter 6 mm). The rod was made from aluminum stock available in the Fysicum workshop and was cut to a length of 60 mm. The aluminum rod was assumed to be of high enough grade to be considered pure and would therefore give approximated results with which to determine if the probe was functioning as expected.
The first data were captured with the following setup. The damping resistors were in parallel and had the values of R_P=1 kΩ and R_S=500Ω. The function generator was set to generate a square wave with an amplitude range of 0-14 V at 10 kHz with a symmetry ratio of 1:1.

The refined procedure, after testing, obtained data by applying a voltage to the primary coil, wait until the eddy currents had diffused out of the sample and then take measurements as the voltage supply was interrupted. The primary coil circuitry was configured so that the function generator, damping resistor and the coil were connected in parallel. A variable resistor was used as the damping resistor. It had a range from 1 Ω to 4 MΩ, and was initially set to 664 Ω. The function generator was set to generate a square wave at 5 kHz and was measured to supply 2.5 V during a 25 μs pulse. The results from this are found in Section 3.1.

2.2 The Coils

Testing the measuring probe required making multiple coils with different parameters in an iterative manner, and so a coil winding rig was designed and constructed, Figure 5. It was equipped to count the number of turns of wire on the coil using an mobile application capable of counting intervals of changing magnetic field strength (Magnetic Field Counter, from Keuwlsoft).

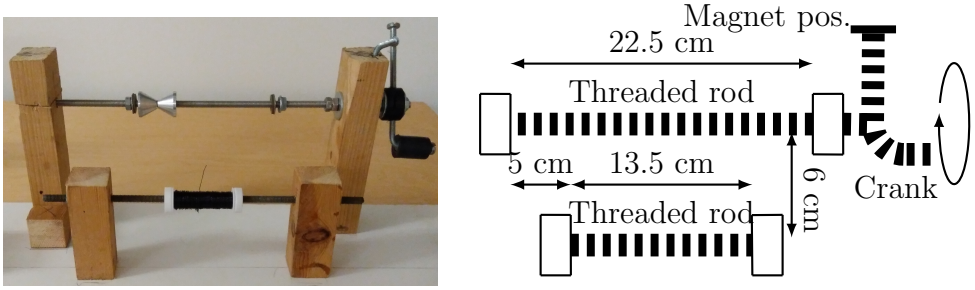

(a) Photo, coil winding rig.

(b) Top view perspective, not to scale. Includes relative distances.

Figure 5: Coil winding rig. Upper threaded rod for securing coil spool with cones tightened with nuts. Lower threaded rod for holding wire spool. The crank on the right hand side was fitted with magnet on one end.

The wire chosen for the coil winding was an insulated copper wire 0.3 mm thick with a resistivity of 1.4 $\mu\Omega$m. It was chosen as the resistance of the wire was considered low enough to not impact the experiment. It was tested to its breaking point with a current supply which showed that the wire started to glow at around 8 A and broke at 9 A, far exceeding the expected operational current of 1 A.

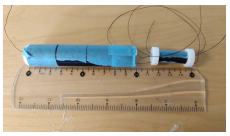

(a) Primary and secondary coil. The ruler is for scale and is 15 cm long.

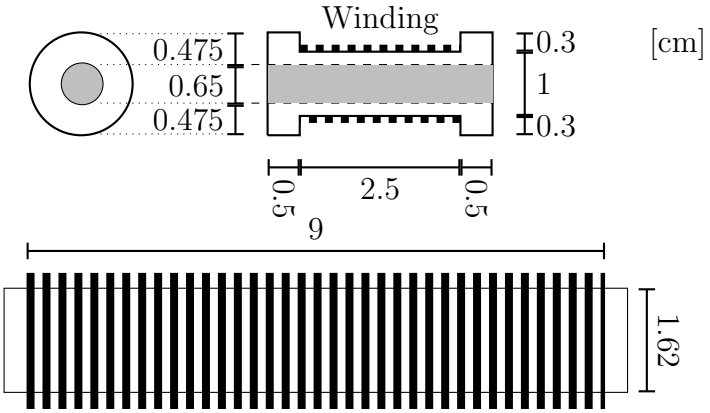

(b) Top, side and front view schematic of the secondary coil to scale. Bottom, front view of the primary coil to scale.

Figure 6: Primary and secondary coils. In (a), the coils with tape are taped down to secure the wire. A 15 cm long ruler is present for scale. In (b), to scale schematics of the two coils.

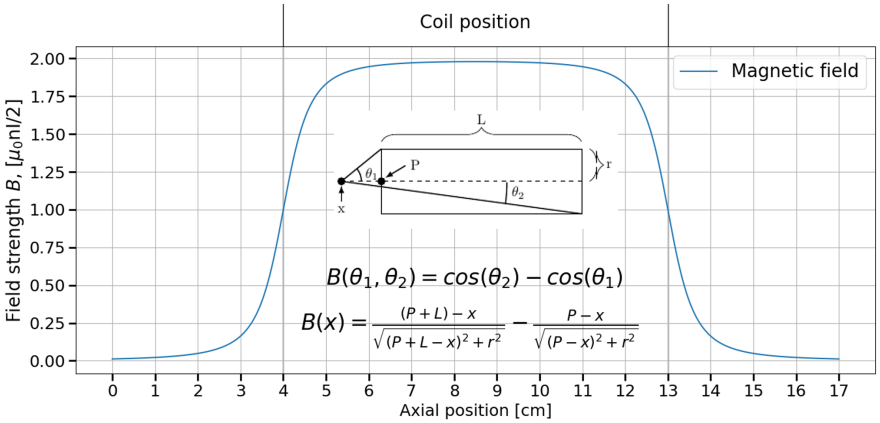

Figure 7: Plot of the calculated field strength generated in the center of the coil. In the expression for the magnetic field strength $B(x)$, $P = 4$ cm is the left edge of the coil, $L = 9$ cm is the coil length, and $r = 0.81$ cm is the coil radius.

To ensure accurate measurement, Hartwig *et al.*[10] showed that the full length of the sample had to be sufficiently affected by the generated magnetic field. From calculations of the magnetic field strength inside a coil (Figure 7), it was seen that a coil length 2 cm longer than the sample would satisfy this condition, Figure 7. This required the coil to be longer than 8 cm as the sample was 6 cm.

A length of PVC (Polyvinyl chloride) plastic tube was used as the spool form for the first test primary coil; it was 96 mm in length, with an inner diameter of 16.2 mm. The winding covered 90.4 mm of the tube which equated to a turn density of n=29.28 cm^{-1}. Given these parameters, to ensure that the sample experienced a nearly homogeneous field its edges should be inside the coil by more than 1 cm. It was tested with a current of 1 A running through it for 1 minute and did not generate any significant amount of heat. It was calculated, using $B = \mu_0 nI/2$, that the generated magnetic field in the middle of the coil with $I = 1$ A current would be 0.3 mT.

When it came to designing the secondary coil it was estimated using Equation 12, where ϕ is the magnetic flux through the cross-sectional area of the coil, $B = B_0 e^{-t/\tau}$, $t = \tau = 72$ μs and the initial field density, B_0, of 0.3 mT that if a signal of 100 mV was desired, then at least 70 turns are required.

$$V = -N\frac{d\phi}{dt} = -N\pi r^2 \frac{dB}{dt} = \frac{B_0 N \pi r^2}{\tau} e^{-t/\tau} \tag{12}$$

The calculations assumed the diameter of the pickup coil to be 1 cm and the current through the primary coil to be 1 A. A spool was lathed out of PE (polyethylene) plastic to hold the sample rod inside it so that when it was placed inside the primary coil it would keep all parts coaxial (Figure 6).
This version of the pickup coil was wound with the same wire as the primary coil and had 77 turns on it. The secondary coil circuitry was also set up in a parallel configuration with the coil, variable resistor box and oscilloscope all in parallel.

(a) Picture of wound differential secondary coil.

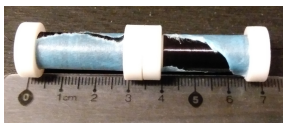

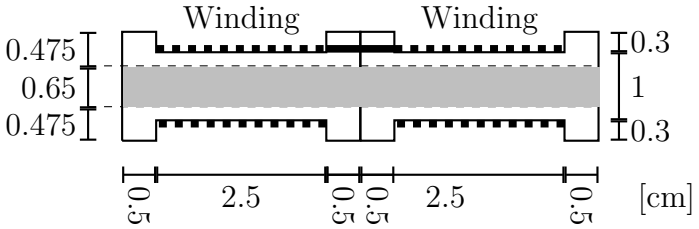

(b) Schematic of the differential secondary coil

Figure 8: Differential secondary coil. These are connected sections of coil with one section wound clockwise and the other counter-clockwise.
(a) The tape on winding is to secure the wire in place and prevent unspooling. The ruler is present for scale.
(b) Schematic of the differential secondary coil, to scale. The shaded area marks hollow volume for sample placement.

Improved design

To improve the previous design, and reduce the induction effect between the primary and secondary coil, a DSC (Differential Secondary Coil) was made. To this end, another plastic spool was lathed with the same dimensions as the previous secondary coil spool. The two pieces of plastic spool were wound with the same wire as used previously (0.3 mm copper wire) and the wire ran continuously though the two sections, Figure 8. The two sections had 77 turns and 74 turns of wire on the windings respectively.

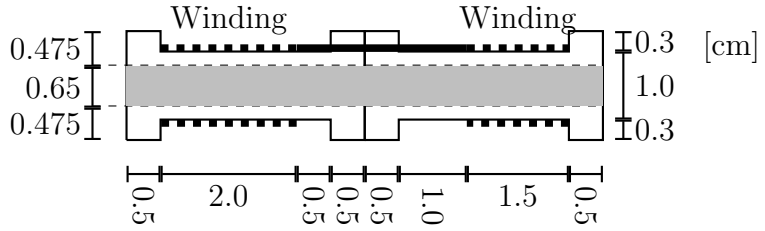

Figure 9: Differential secondary coil schematic with dissimilar numbers of turns on each section, and with the sections further apart.

A second design of the DSC was made to improve the probe performance. The DSC was rewound to have a dissimilar amount of turns in each section as it was noted that one section was always closer to the edge and protruding out of the primary coil where the field flux was less. The second DSC was wound with 0.22 mm wire, the first section was 20 mm long with 79 turns, then a 25 mm gap and the second section had 53 turns spanning 15 mm (Figure 9). This alteration was found to aid the consistency of the measurements since the section with the sample was now closer to the center of the primary coil, results in Section 3.2.1.
Ultimately, a new primary coil with a thinner wire was constructed. This wire, 0.22 mm lacquered copper wire, on the primary coil form could accommodate a higher number of turns and so increase the magnetic field strength. The new primary coil had 358 turns running over a length of 79 mm. This coil was tested with the modified DSC, Section 3.2.2.
The proximity of the primary coil to the DSC and the sample could have some effect on the measurements. With this in mind, a new primary coil was designed with a larger diameter (38 mm), increasing the distance between the coils. It was wound with the 0.22 mm lacquered copper wire spanning 61 mm with 240 turns. The results found was made with the first iteration of the DSC (Section 3.2.3).

2.3 Testing

The primary coil circuitry was tested by varying the wave functions, the damping resistor strength and placement. This extensive testing provided data indicating that the circuit is more stable with the damping resistor in series. The oscillations in the voltage signal from the secondary coil were noticeably smaller when the primary coil damping resistor was in series instead of in parallel.
This was tested using the circuit shown in Figure 10. The test showed that the current through the primary coil had an amplitude of 80 mA and it reduced from max amplitude to zero in 8 μs.

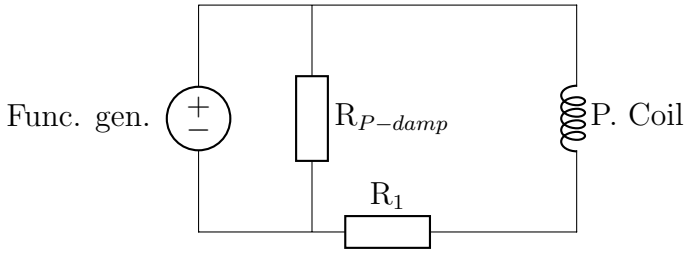

Figure 10: Circuit diagram for the primary coil circuit during testing of current through coil. Function generator supplying a square wave at 10 kHz, daming resistor $\mathbf{R}_{P-damp}$=1 kΩ and the control resistor $\mathbf{R}_1$ assumed values between 1 - 700 Ω.

The extended current decay through the primary coil was not desirable, as it blurs the diffusive decay of the eddy current in the sample. By shifting to a series configuration (Figure 11), the decay time for the primary coil current can be reduced to 1 μs. This also resulted in the current being $\sim$17 mA because of the increase of resistance from the damping resistor in the circuit.

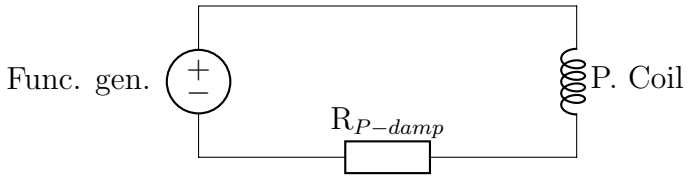

Figure 11: Circuitry for the modified primary coil circuit with damping resistor $\mathbf{R}_{P-damp}$= 700 Ω.

3 Results

3.1 Differential Secondary Coil

During the course of this project, I designed and built a eddy current probe by extending on the original work done by Bean *et al.* [1]. The operation of the Bean setup was tested, see Figure 12(a), and found to be unsuitable for measuring eddy current dissipation. This is because there is a large induced signal in the secondary coil (lower trace) from the primary coil, making it difficult to identify the effect of eddy current dissipation. This is the same kind of induction mechanism as seen in electrical transformers.

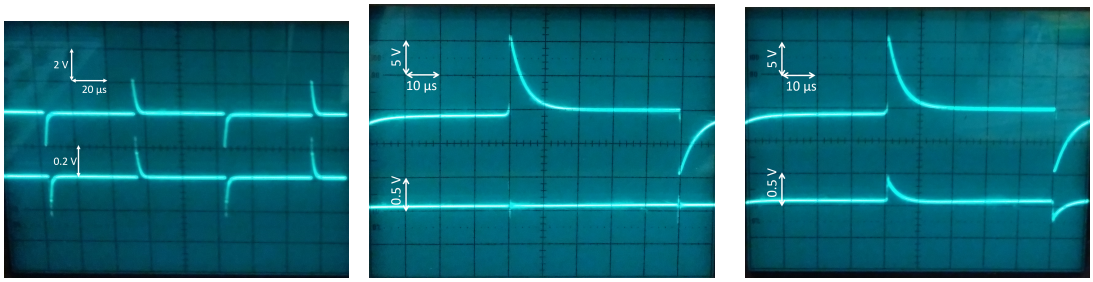

(a) Bean setup, without sample

(b) DSC setup, without sample

(c) DSC setup, with Al rod sample

Figure 12: Ocsilloscope readout. Upper trace: The primary coil circuit voltage. Lower trace: The secondary coil circuit voltage, circuit from which the measurement data is extracted. Time and voltage divisions are indicated in figures.

In order to counteract the induction between the coils, the circuit was redesigned to use a Differential Secondary Coil (DSC). The improved performance of that setup is shown in Figure 12(b), where the induced signal is very faint.
An aluminum (Al) rod sample was then introduced in the new setup and a distinct eddy current signal is observed, Figure 12(c). The eddy current observed is on the order one tenth of the current supplied to the primary coil and it would have been difficult to make measurements with this implementation of the design suggested by Bean.
The measurement of diffusing eddy currents for the purpose of getting the resistivity is only valid after the current in the primary coil is gone as the eddy currents are continuously diffusing and induced during the process of changing magnetic flux, [10]. From Figure 12(c) it is clear that the eddy currents are diffusing on a

similar time scale as the current through the primary coil is subsiding. This made the circuitry inappropriate for data acquisition and further improvements to the setup were required. In the process of improving the sensitivity of the eddy current

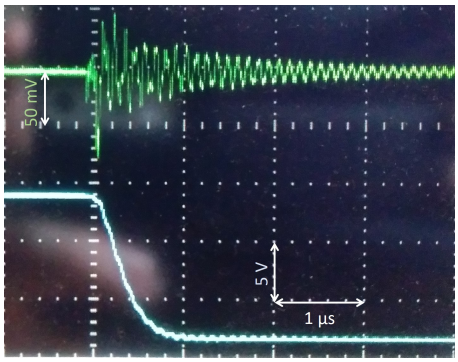

(a) DSC setup, damping resistor in series, without sample.

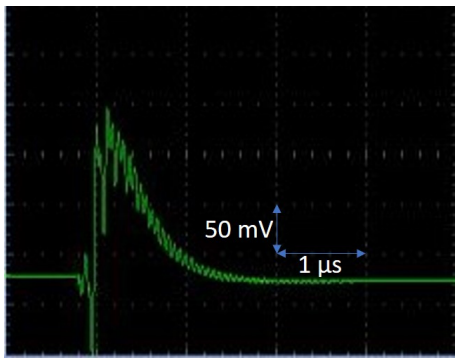

(b) DSC setup, damping resistor in series, with Al rod sample.

Figure 13: Oscilloscope readout. Time and voltage divisions are indicated in figures.
(a) Upper trace: DSC circuit voltage, Lower trace: Primary coil voltage. The current through the primary coil decays to zero within 1 μs.
(b) Trace: DSC cicuit voltage with Al rod sample. The start of initial pulse in primary coil is indicated by initial reaction in DSC trace.

probe, the time constant of the primary coil circuit was investigated. The time it takes for the current in the primary coil to decay should be as short as possible to ensure the maximum amount of eddy currents available for measurement. When the damping resistor on the primary coil was placed in series instead of in parallel, the time it took for the current to decay was shortened by roughly a factor of ten. This is seen when comparing the current reduction time of Figure 13(a) and Figure 12(b) or (c) which was on the order of 8 μs in the previous setup and now on the order of 1 μs.
It can be deduced, from Figure 13(b), that when the current through the primary coil is gone (1 μs after the initial reaction in DSC trace), there is only a very small signal remaining from the eddy currents in the sample to measure. The resulting data were analyzed by fitting a exponential decay curve. The time constants varied with $\tau = 3.16 \pm 0.13$ μs giving a resistivity of $(6.20 \pm 0.25)^{-7}$ Ωm, from Equation 5. These values are greater than the tabulated value of $2.7 \cdot 10^{-8}$ Ωm. The suspected reason for this discrepancy is the lack of sufficiently induced eddy currents which is dependent on the amount of current through the primary coil.

3.2 Further designs of the eddy current probe

As the setup was operating at maximum power, an increase in the number of turns on the primary coil increases the maximum magnetic field strength and therefore increases in induced current. A sample position closer to the center of the primary coil would also improve the induction as the sample was off center where the magnetic field is not locally homogeneous as Hartwig [10] showed to be important.

3.2.1 Influence of DSC section separation and sample position relative to primary coil.

The DSC works on the principle of two equal and opposing voltages which are generated by a changing magnetic field. The DSC must be situated such that the two sections experience the same amount of change in the magnetic field, meaning that the DSC in our case is situated in the center of the primary coil. That, in turn, means that the individual sections of the DSC are positioned off center, relative to the primary coil.
We now discuss two cases that can affect the performance of the DSC:

- Case 1: The mutual interference of the coils of the DSC
- Case 2: The sample position with respect to the primary coil

Case 1:
The proximity of the two section of the DSC to each other interferes with the results since the magnetic field generated by the section without a sample extends to some degree to the other and does influence the induced eddy currents. This extension is illustrated by Figure 7, where the field strength is non-zero beyond the edges of the coil. With this in mind, the DSC was rewound with a gap of 25 mm between the two sections to minimize the effect the sections have on each other.
Case 2:
The magnetic field generated by the primary coil drops off rapidly at the edges but can be considered homogeneous closer to the center of the coil, as illustrated by Figure 7. The sample should be placed in such a way that it is saturated by a virtually homogeneous field in order to eliminate any effects that might alter the results, as mentioned by Hartwig *et al*. [10]. The DSC was thus redesigned to have different number of turns for the two sections, one section with 79 turn and the other with 53. In Figure 14, the result from the aforementioned modifications can

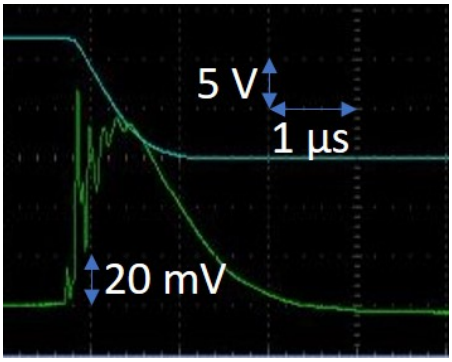

Figure 14: Redesigned DSC setup, damping resistor in series. Upper trace: Primary coil circuit voltage, current decays in $\sim$ 1.2 μs. Lower trace: DSC circuit voltage.

be seen, using the redesigned primary coil with 358 turns. The initial oscillations in the DSC trace are similar to previous setups but a significant difference can be seen in the decay of the eddy current. The signal from the dissipating eddy currents is now free from oscillations.
Despite the improved signal, the calculated resistivity, using the same method as previously, was comparable to previous results at $4.96{\cdot}10^{-7}$ Ωm (expected resistivity of aluminum $2.7{\cdot}10^{-8}$ Ωm). This furthers the suspicion of the need for larger currents in the primary coil in order to induce greater amounts of eddy current in the sample.

3.2.2 Influence of wire gauge

A increase in the amount of eddy currents induced is desired as it would allow for more accurate measurements. This should be achieved by increasing the magnetic flux while retaining the same time of current cancellation, requiring the setup to be less sensitive.
To do this, the primary coil was rewound with a narrower gauge of wire (diameter 0.22 mm as opposed to 0.38 mm), to increase the number of turns on the spool (from 265 to 358). This increases the density of turns, n, and if the current amplitude is conserved then the magnetic field strength, B, in the center of the coil increases linearly with n, ($B = \mu_0 nI/2$, Griffiths [3]).
When the number of turns on the primary coil is increased, the capacitance of the primary coil also increases. This can be seen in Figure 15 as the longer decay time of the current through the primary coil which now has increased to about 1.2 μs.

The data were analyzed, as before, by fitting a exponential curve. The range of time constants recovered was between 3.43 and 4.03 μs resulting in a resistivity range between $4.85{\cdot}10^{-7}$ and $5.69{\cdot}10^{-7}$ Ωm. Again, comparing to the expected resistivity of aluminum, $2.7{\cdot}10^{-8}$ Ωm, shows that these results are larger but it is an improvement when compared to the previous range of $5.94{\cdot}10^{-7}$ to $6.45{\cdot}10^{-7}$ Ωm.

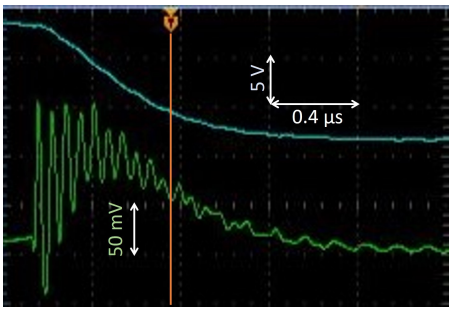

Figure 15: DSC setup, damping resistor in series, with Al rod sample. Data from measurement after rewinding of primary coil. The vertical line is the trigger line. The upper trace is the primary coil circuit voltage and the lower trace is the DSC circuit voltage. The current through the primary coil has a decay time $\sim$ 1.2 μs.

3.2.3 Influence of primary coil diameter

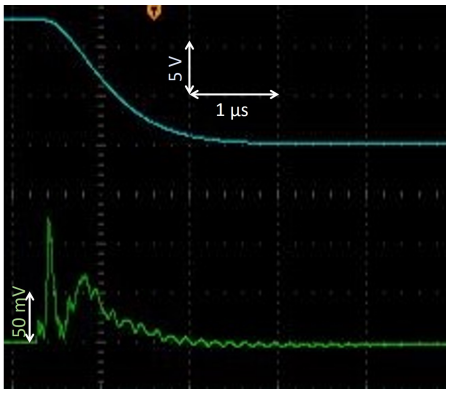

Figure 16: Oscilloscope readout from the 38 mm diameter, primary coil (upper trace) and DSC (lower trace). The initial interference between primary and secondary coil is seen as the large peak at start of DSC trace. The current through the primary coil takes longer time to decay to zero than for smaller the diameter coils, $\sim$ 2.5 μs.

Finally I examine the effects of effective capacitance between the coils on the data. The primary coil was rewound on a spool of larger diameter, 38 mm, with a 0.22 mm gauge wire and had 240 turns. In Figure 16, the current through the primary coil (upper trace) decays in roughly 2.5 μs, which is longer than for the coil with a smaller diameter.
The initial effects from the pulse are reduced compared to the previous setup employing a primary coil of smaller diameter. This is seen in Figure 16 where the initial peak drops very quickly, giving way to the eddy current dissipation behavior.
It can also be seen in Figure 16 that the maximum amount of dissipation is at the greatest decline of current in primary coil. This is expected as the amount of current induced in the sample is related to the rate of change of current in the primary coil.

4 Discussion

When looking at the data it can be seen that only a small amount of eddy current is left when the current in the primary coil is gone, making the extraction of the resistivity difficult. Bean *et al.* [1] theorized that the eddy current dissipation behaved according to a infinite sum of exponentials, where the higher order exponents have increasing orders of time constants, making the higher order exponentials decay very fast and the behavior of dissipation converges to a single exponent described in Equation 5.
It can be concluded that the data retrieved is from the decay of the higher order exponentials described by Bean *et al.* [1], resulting in a larger time constant and thus implying that the resistivity is lower. The most probable way of solving this is to increase the induced eddy currents to a much higher degree, promoting the decay of the higher order exponentials before the zeroth order exponential becomes to small for measuring.
I suspect that the better performance of the original design by Bean is due to differences in power supply and the delivery of that power. The time frame of this project only allowed access to a commercial function generator. Due to the generator specifications (max output no load: 20 V, rise and fall times: < 35ns), the power supply provides a limited amount of current to the primary coil. Bean *et al.* used a customized current supply with switches, allowing more current to pass through the primary coil and in turn induces more eddy currents in the sample.

From the measurement made by the later configuration and versions of the coils, it was seen that the fitted value of τ ranged from 3 to 4 μs. This is significantly smaller than the value expected for the known resistivity of aluminum, 70 μs.
The measurements where the current through the primary coil rapidly decrease to zero, in a little over 1 μs, showed that the induced eddy currents diffuse in a similar span of time. This means that the eddy currents after the initial pulse of current through the primary coil are already greatly reduced and do not present a data set reliable enough to be used in the deduction of the resistivity. The current pulse used in Prance [5] went from max to zero in roughly 0.5 μs which is on the same order, but he had a current source with switch controlling the interruption of the supplied current to the primary coil.
The differential secondary coil did eliminate most of the interference arising from the initial pulse coming from the primary coil as intended. However, Bean *et al.* [1] did not mention any use or need for such a coil. Again, the suspicion is that the current supply was not great enough in our setup.
Rewinding the coils with thinner wire gave the opportunity to produce a larger magnetic field density in the primary coil and pick up more in the case of the secondary coil. An undesirable consequence for the primary coil was that the time it took for the current to recede increased by a fraction and caused and increased difficulty in the measurement of the diffusing eddy currents.
The winding of a primary coil with a larger diameter appeared to give less interference with the secondary coil and a more stable signal from the same. This is considered to be an effect related to the magnetic field lines not being homogeneous close to the wiring. Further from the wires on the coil and closer to its center, the field lines are more coaxial and straight which is a premise of the measuring probe.
The greatest improvement of the data came from the redesign of the DSC by increasing the separation between the two sections of the coil. This alteration eliminated the interference the two section had on each other. The interference arises from the magnetic fields in the individual sections interacting, resulting in a oscillation in the measured voltages from the DSC circuit.

5 Conclusion

In conclusion, this experiment has found some insight into the workings and failings of the measuring probe using a contactless method.
In the process of trying to improve the quality of the measurements, different variables were considered, tested and found to have little or no impact on the amount of induced eddy current. The variables included were coil parameters (diameter and number of turns), and wire diameter.
This process highlighted the variables and their individual roles when considering the impact they had on the probe but it did not exclude them. If more variations of the different parameters had been tested, then it might have been possible to exclude some factors from the experimental tuning criterion.
The final speculation is that the amount of induced eddy currents in the sample has to be far greater than I was able to produce with my setup. This is hypothesized because of the diffusive nature of the eddy currents. As soon as they are induced, they start to diffuse and if the change in magnetic flux is not strong enough they will dissipate fast and leave little to nothing left for measuring. Although this experiment did not succeed in producing a working measuring probe, I have explored various design choices, in particular the DSC, and confidence in the method is not reduced. Many before me have shown that this is a viable method of determining the resistivity of a sample.

Acknowledgements

I would like to thank, in general, Lund University from supplying the needed equipment for this project and the experiment. The staff scattered around different departments that has help me in retrieving components, equipment and material, specifically Håkan Ivansson, Tommy Holmqvist and Stanley Micklavzina. My supervisor, Elizabeth Blackburn, deserves more than my gratitude as she not only has supported this project throughout its course but also me and my demanding nature. The synchrotron radiation division, for providing me with work spaces in the form of an office and a lab in which to conduct my experiment. On a personal note, I will acknowledge my family for their support, especially my father, Bengt Klintrup, and my sister, Erika Klintrup Gustafsson.

References

[1] Bean, C., DeBlois, R., & Nesbitt, L. (1959). *EddyCurrent Method for Measuring the Resistivity of Metals.* Journal Of Applied Physics, 30(12), 1976-1980. https://doi.org/10.1063/1.1735100

[2] Hofmann, P. (2015). *Solid state physics* (2nd ed., p. 79 - 81). Wiley-VCH Verlag GmbH & Co. KGaA. Weinheim, Germany.

[3] Griffiths, D. (2017). *Introduction to electrodynamics* (4th ed., p. 296 - 298). Pearson Education Inc. Cambridge, United Kingdom

[4] Cochran, J., & Mapother, D. (1958). *Superconducting Transition in Aluminum.* Physical Review, 111(1), 132-142. https://doi.org/10.1103/physrev.111.132

[5] Jonathan Prance, *Flux Lines in Superconductors*, MSc Thesis, University of Birmingham, UK (2004)

[6] Cutkosky, R. (1964). *Four-terminal-pair networks as precision admittance and impedance standards.* IEEE Transactions On Communication And Electronics, 83(70), 19-22. https://doi.org/10.1109/tcome.1964.6539563

[7] Kraftmakher, Y. (2000). *Eddy currents: Contactless measurement of electrical resistivity.* American Journal Of Physics, 68(4), 375-379. https://doi.org/10.1119/1.19440

[8] Wejgaard, W., & Tomar, V. (1974). *Contactless measurement of electrical resistivity by eddy current methods: discussion and a new technique.* Journal Of Physics E: Scientific Instruments, 7(5), 395-399. https://doi.org/10.1088/0022-3735/7/5/027

[9] Delaney, J., & Pippard, A. (1972). *Electrodeless methods for conductivity measurement in metals.* Reports On Progress In Physics, 35(2), 677-715. https://doi.org/10.1088/0034-4885/35/2/304

[10] Hartwig, K., Hua, C., & McDonald, L. (1991).*Effect of primary coil size on eddy current decay resistivity measurements.* Cryogenics, 31(3), 153-158. https://doi.org/10.1016/0011-2275(91)90168-v

[11] Young, H., & Freedman, R. (2015). *Sear's and Zemansky's university physics* (14th ed., p. 996). Pearson Education. Harlow, Essex.

[12] Appendix B: Material Properties. (2016), 635-642. https://doi.org/10.1002/9781118936160.app2

[13] LePage, J., Bernalte, A., & Lindholm, D. (1968). *Analysis of Resistivity Measurements by the Eddy Current Decay Method.* Review Of Scientific Instruments, 39(7), 1019-1026. https://doi.org/10.1063/1.1683554

[14] Alphonce, R., & Pilström, H. (2011). *Formler och tabeller från Natur och kultur* (2nd ed., p. 72). Natur och kultur.